THE ASTROPHYSICAL JOURNAL, 475:823–828, 1997 February 1

THE *ASCA* X-RAY SPECTRUM OF THE UNUSUAL BINARY LSI +61°303

DENIS A. LEAHY
Department of Physics, University of Calgary, Calgary, Canada T2N 1N4; leahy@iras.ucalgary.ca
FIONA A. HARRISON
Division of Physics, Mathematics, and Astronomy, California Institute of Technology, Pasadena, CA 91125; fiona@citsrl.caltech.edu
AND
ATSUMASA YOSHIDA
Institute of Physical and Chemical Research, Saitama 351-01 Japan; ayoshida@postman.riken.go.jp
Received 1996 April 4; accepted 1996 August 13

ABSTRACT

The unusual Be binary LSI +61°303 was observed by the *ASCA* X-ray satellite twice during the 26 day orbital-outburst cycle. Here we present the results of the spectral analysis of the *ASCA* data. The emission spectrum can be characterized by an absorbed power law and is inconsistent with other single-component models such as blackbody or hot plasma emission. The data show both flux and spectral variability between the two observations. The column density is determined for LSI +61°303 , and we put upper limits on Fe line emission and Fe absorption edge optical depth. The power-law index is similar to that seen for classical X-ray pulsars; however, the low X-ray luminosity and the power-law emission in other wavebands indicate that the emission is not from an optically thick accretion column but rather synchrotron or inverse-Compton emission from relativistic particles. We argue that the sub-eV emission is synchrotron, the super-eV emission is inverse Compton and that the magnetic field in the emission region is a few hundred gauss.

Subject headings: binaries: spectroscopic — radio continuum: stars — stars: individual (LSI +61°303) — stars: neutron — X-rays: stars

1. INTRODUCTION

LSI +61°303 is one of a small but important group of radio-emitting X-ray binary systems. Well-known members of this class include SS 433, Cyg X-1, Cyg X-3 and Circinus X-1. Considerable interest has centered around LSI +61°303 since 1977 when it was discovered to be a strong, variable radio source (Gregory & Taylor 1978) and proposed to be the counterpart of the *COS-B* γ-ray source 2CG 0135+01. It was soon identified with its Be star optical counterpart (Gregory et al. 1979). The radio light curve exhibits outbursts the periodicity of which corresponds to the optical periodicity of the orbital motion (Hutchings & Crampton 1981).

LSI +61°303 has been also identified as an X-ray (Bignami et al. 1981) and possibly an MeV γ-ray source (van Dijk et al. 1993). It was possibly detected in high-energy (500 keV–1 MeV) X-rays (Perotti et al. 1980); however, these results are inconsistent with other spectral information (see discussion in § 4.1 below).

Here we present the results of the analysis of the *ASCA* images and X-ray spectra of LSI +61°303. Analysis of the time variability and simultaneous radio observations of LSI +61°303 are presented in a following paper (Harrison, Leahy, & Waltmann 1996).

2. OBSERVATIONS

LSI +61°303 was observed by *ASCA* (Tanaka, Inoue, & Holt 1994) during two portions of the same 26 day cycle. *ASCA* has four identical thin foil light-weight X-ray telescopes which focus X-rays onto one of two solid state imaging spectrometers (SIS) or one of two gas imaging spectrometers (GIS). Hereafter the two SIS are referred to as SIS0 and SIS1, and the two GIS as GIS2 and GIS3.

The first pointing took place on 1994 February 3 (MJD 49386) starting at 1:45 UT and ending at 11:01 UT, corresponding to radio phase 0.2. The second pointing took place on 1994 February 9 (MJD 49392) starting at 7:34 UT and ending at 17:08 UT, corresponding to radio phase 0.42. Binary radio phase was calculated using the 26.496 day arbitrary ephemeris of Taylor & Gregory (1984). The first pointing will be referred to as P1 hereafter, and the second pointing as P2. For P1, the SIS0 and SIS1 net exposure times were 18843 and 18803 s, respectively; the GIS2 and GIS3 exposure times were both 17961 s. For P2, the SIS0 and SIS1 times were 33645 and 33639 s, respectively; the GIS2 and GIS3 times were 19344 and 19347 s.

All of the CCD (SIS0 and SIS1) observations were taken in faint mode (2 CCD mode for the first pointing and 1 CCD mode for the second pointing). The data processing was carried out at the Institute of Physical and Chemical Research, Tokyo, using the *ASCA* reduction software and a standardized set of reduction methods. This included filtering the data to remove hot pixels from the CCD data and observation intervals with high background (i.e., telescope pointings close to Earth's limb or after SAA passage).

3. ANALYSIS AND RESULTS

3.1. *X-Ray Image*

The GIS2 image for the second pointing (P2) is shown in Figure 1 in contour map form, labeled with 1950 coordinates. LSI +61°303 is the bright source near the center. The position is consistent with the published position of R.A. 40°.115, decl. +61.235 (J2000) (Gregory et al. 1979).

There is a second point source 7′ southwest of LSI +61°303. This source is seen in the same location in all of the GIS images (both detectors, both pointings). It is not seen in the SIS images, as it is just outside of the SIS field of view. Hereafter, this source is referred to as source 2. The position of source 2 corresponds to R.A. 39°.976, decl. +61.128 (J2000), with an accuracy of 0°.004.

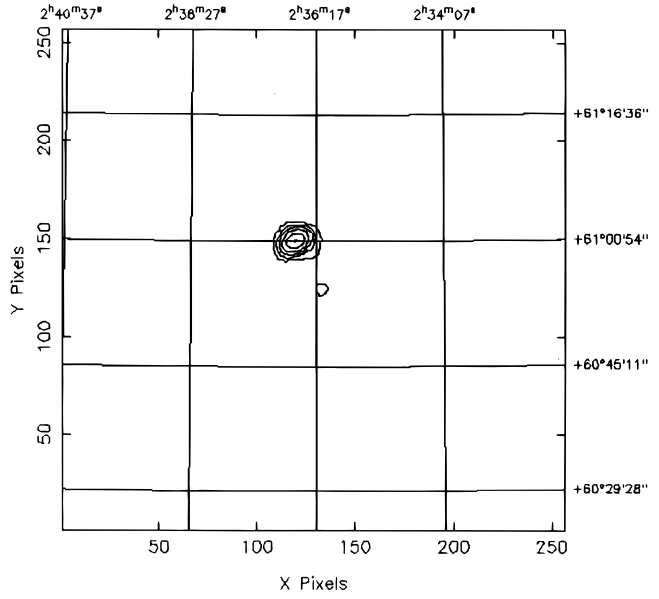

FIG. 1.—*ASCA* GIS2 1994 Feb 9 exposure (19343 s) contour map of the LSI +61°303 field.

3.2. *Spectrum Analysis*

For LSI +61°303 spectra were extracted from the event files for both pointings. For the SIS detectors, the source and background regions were taken approximately 3′.2 in radius. For the GIS detectors the regions were 4′.9 in radius. For source 2, seen only in the GIS detectors, the source region was 3′.4 in radius. The background-subtracted count rates for the two pointings and the two sources (LSI +61°303 and source 2) are given in Table 1. This shows that both sources are highly significant detections.

The resulting SIS0 and SIS1 spectra were rebinned from 4096 to 512 spectral channels. Then all (SIS and GIS) spectra were further rebinned to have minimum 20 counts per bin, so that a χ^2 statistic for fitting is applicable. The highest channels, which were consistent with zero counts, were ignored in the spectral fits. This resulted in spectra with about 120 channels with 20 or more counts for LSI +61°303 and with about 40 channels with 20 or more counts for source 2.

Spectral fits were made using power law, Raymond-Smith, and blackbody models. For all models parameter 1 (hereafter param1) is column density and param3 is the normalization. For the blackbody and Raymond-Smith models param2 is temperature in keV units; for the power-law model, param2 is the power-law index. The power-law model is referred to as "power," the Raymond-Smith model as "raym," and the blackbody model as "bbdy." χ^2_r is the reduced χ^2 value of the fit.

3.3. *ASCA Spectra of LSI +61°303*

The observed spectrum for LSI +61°303 from the SIS0 detector for P1, with the best-fit power-law model spectrum is shown in Figure 2. Figure 3 shows the GIS2 for P1 spectrum and best-fit power-law model. These power-law fits are statistically acceptable, as are the fits using the Raymond-Smith model. However, the blackbody fits are significantly worse and are rejected on this basis and also because the implied column density is unacceptably low. The Raymond-Smith model gives slightly higher χ^2_r values than the power law and also gives significantly lower column densities and high temperatures (of order 10–20 keV).

The four spectra for each pointing (SIS0, SIS1, GIS2, and GIS3) were fitted simultaneously with a single model (referred to as joint fits). Table 2 shows the results of joint fits for both LSI +61°303 and source 2 (source 2 only has GIS2 and GIS3 spectra and is discussed below). Again the blackbody had higher χ^2_r and unacceptably low column

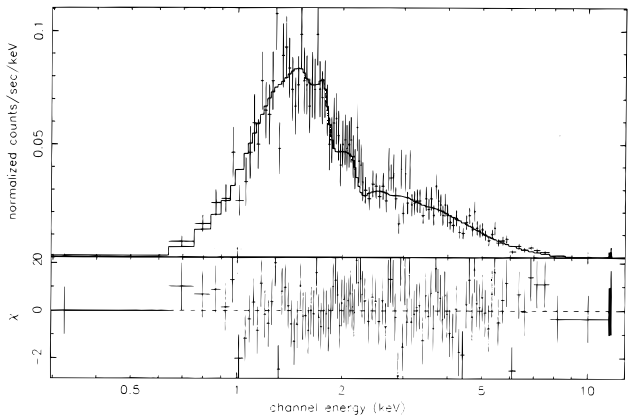

FIG. 2.—*ASCA* SIS0 spectrum of LSI +61°303, first pointing, with power-law model spectrum.

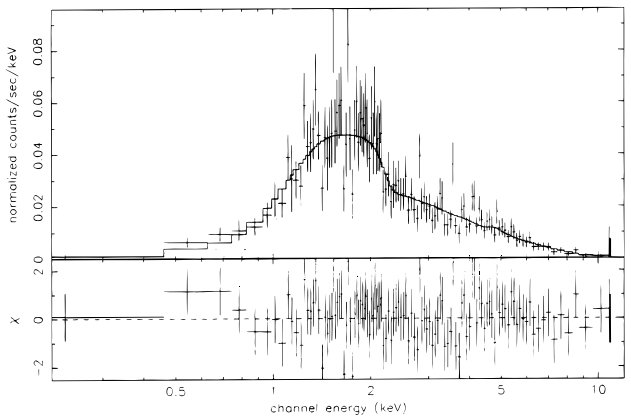

FIG. 3.—*ASCA* GIS2 spectrum of LSI +61°303, first pointing, with power-law model spectrum.

TABLE 1

BACKGROUND-SUBTRACTED COUNT RATES (count s^{-1})

Source	SIS0 Count Rate	SIS1 Count Rate	GIS2 Count Rate	GIS3 Count Rate
LSI P1	0.1622 ± 0.0034	0.0797 ± 0.0025	0.1269 ± 0.0035	0.1253 ± 0.0034
LSI P2	0.0891 ± 0.0023	0.0648 ± 0.0019	0.0938 ± 0.0023	0.1115 ± 0.0025
Source 2 P1.....	n/a	n/a	0.0160 ± 0.0015	0.0128 ± 0.0014
Source 2 P2.....	n/a	n/a	0.0169 ± 0.0011	0.0166 ± 0.0011

TABLE 2

SPECTRAL PARAMETERS FOR JOINT FITS TO SPECTRA

Model	Param1[a]	Param2[a]	Param3[a]	Flux(2–10)[b]	Flux(0.5–2)[b]	χ_r^2
			LSI, P1			
SIS0+SIS1+GIS2+GIS3:						
Power	0.544–0.670	1.63–1.78	$1.43–1.74 \times 10^{-3}$	6.05×10^{-12}	1.17×10^{-12}	1.31
Raym	0.369–0.439	13.1–21.0	$4.47–4.80 \times 10^{-3}$	6.64×10^{-12}	1.15×10^{-12}	1.44
Bbdy	0.00–0.034	0.911–0.960	0.615–0.734	4.35×10^{-12}	1.11×10^{-12}	1.81
			LSI, P2			
SIS0+SIS1+GIS2+GIS3:						
Power	0.532–0.645	1.75–1.90	$1.21–1.45 \times 10^{-3}$	4.25×10^{-12}	9.67×10^{-13}	1.20
Raym	0.355–0.428	8.18–11.3	$3.29–3.47 \times 10^{-3}$	4.65×10^{-12}	9.48×10^{-13}	1.32
Bbdy	0–0.029	0.829–0.869	0.638–0.752	2.88×10^{-12}	9.41×10^{-13}	1.73
			Source 2			
P1+P2,SIS1+GIS2:						
Power	0–0.036	3.02–3.46	$2.74–3.36 \times 10^{-4}$	1.43×10^{-13}	7.53×10^{-13}	1.05
Raym	0.398–0.673	0.666–0.872	$5.11–8.61 \times 10^{-4}$	6.65×10^{-14}	4.13×10^{-13}	1.12
Bbdy	0–0.025	0.230–0.273	9.58–24.0	2.55×10^{-14}	4.94×10^{-13}	1.62

[a] 90% confidence range given; see text for description of parameters.

[b] 2–10 keV or 0.5–2 keV flux in ergs cm^{-2} s^{-1} given for the best-fit model spectrum.

density, so it can be rejected. The Raymond-Smith spectra have higher χ_r^2 and lower column density than the power-law fits and again show high temperatures. The power-law model is preferred on the basis of χ_r^2 alone, but considering the column density of 10^{22} cm^{-2} to LSI +61°303 measured in radio (Frail & Hjellming 1991), it is the only acceptable spectral model.

The two observations (P1 and P2) are compared. The column densities for P1 and P2 spectra agree. The 2–10 keV flux is 30% lower for P2 than P1, and the 0.5–2 keV flux is 17% lower. The data also indicate a difference in power-law index (or temperature, for the Raymond-Smith model) at about the 90% confidence level: the P2 spectrum is softer (or cooler).

Joint fits to all of the *ASCA* spectra from both pointings were done. The χ_r^2 values were significantly higher than for fits to data from the individual pointings. This can be attributed to the different power-law index (or temperature) for the two pointings. The parameters for the joint fits to both pointings were intermediate between those for P1 and P2, as expected. The blackbody fit was rejected even more strongly.

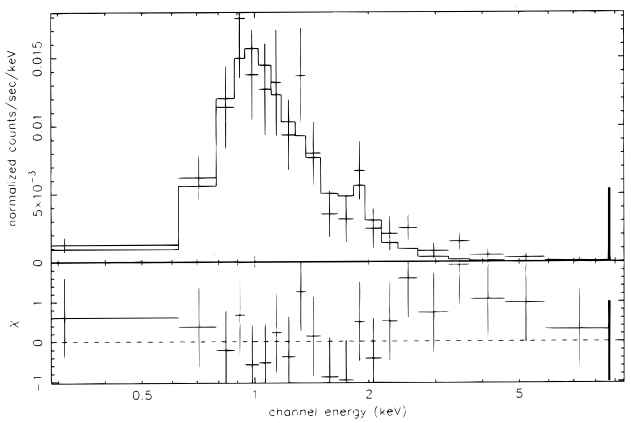

FIG. 4.—*ASCA* GIS2 spectrum of source 2, first pointing, with Raymond-Smith model spectrum.

The observed spectra of LSI +61°303 show no discernable iron emission line at 6.4 keV, nor any iron absorption edge (see Figs. 2 and 3). To put upper limits on iron line emission, simultaneous fits were performed on all the *ASCA* spectra of LSI +61°303 . The fits included a 6.4 keV (0.1 keV width) iron emission line in the model and a power-law continuum with all parameters freely variable. The 90% upper limit for the iron line intensity of 9×10^{-6} photons cm^{-2} s^{-1} was derived. This is equivalent to a 90% upper limit on equivalent width of 130 eV. Similarly, a 3 σ upper limit on optical depth of a 7.1 keV iron edge was found to be 0.51. The 3 σ upper limit to optical depth of a 8.5 keV broad iron edge (1 keV smeared) is 3.1.

3.4. *ASCA Spectrum of Source 2*

The observed spectrum for source 2 from the GIS2 detector for P1, with the best-fit Raymond-Smith model spectrum is shown in Figure 4. The number of counts for source 2 is significantly less than for LSI +61°303. Even so, the blackbody model has significantly worse χ_r^2. The power-law and blackbody spectra give very low column densities. This fact, together with the steep power-law index, is a strong indication that the Raymond-Smith model is a better spectral model than a power law and is significantly better than blackbody.

The P1 and P2 spectra for source 2 were consistent with having the same spectral parameters. Thus, joint fits were carried out including P1 and P2 spectra. The power-law and Raymond-Smith models both gave statistically acceptable fits. The last entry of Table 2 gives the resulting 90% limits on the spectral parameters. The Raymond-Smith spectral model is preferred here since the power-law model gives a very low column density and very steep spectral index.

4. DISCUSSION

4.1. *LSI +61°303*

The *ASCA* instruments observed LSI +61°303 during two pointings at binary phases 0.2 and 0.42. Spectral fitting rules out the blackbody model by the large χ_r^2 and the

unrealistically low fit N_H. The Raymond-Smith hot plasma model is also unlikely: the fits have a higher χ_r^2 than the power-law model, the derived plasma temperature is very high, and, more importantly, N_H is inconsistent with the radio-derived value (Frail & Hjellming 1991). Thus, the power-law model is the only consistent model for the observed spectra. We note that our power-law fit to the *ASCA* data is consistent with the *ROSAT* PSPC spectrum of LSI +61°303 (Goldoni & Mereghetti 1995; Taylor et al. 1996; Harrison & Leahy 1996).

The power-law index is in the range 1.6–1.9, similar to that seen for classical X-ray pulsars. The classical accreting X-ray pulsars are high luminosity and also show iron line emission. Since the *ASCA* spectra of LSI +61°303 show no evidence for Fe line emission, and the X-ray luminosity is low (4.7×10^{33} ergs s^{-1}), LSI +61°303 is not a classical pulsar. However, some other Be X-ray binaries such as X Per (Schlegel et al. 1993) also have low luminosity and show no iron line.

N_H is now well determined to be $5.5–6.5 \times 10^{21}$ cm^{-2} (90% confidence), which is currently the best determination, and avoids the assumption on spin temperature (e.g., Spitzer 1978, p. 42) needed for determination of column density from radio observations. The constancy of N_H for the two pointings shows there is no significant column density change with orbital phase, as might be expected if there was absorption in the wind of the Be star. We have also obtained a limit on the presence of an iron absorption edge, which limits the absorbing column density of ionized matter.

In Figure 5, the X-ray and γ-ray spectra of LSI +61°303 are summarized an a $\nu - F_\nu$ plot (for which equal luminosity per decade of frequency is a horizontal line). The P1 and P2 *ASCA* spectra, and the measurements reported from the MISO balloon (Perotti et al. 1980), Comptel (van Dijk et al. 1993), *COS-B* (Swanenburg et al. 1981), and EGRET (Thompson et al. 1995) experiments are shown. The 2–10 keV flux is 30% lower in the second pointing. There is a difference in spectral index between the two pointings at the 90% confidence level, with P2 (phase 0.42) having the steeper spectrum (1.83 vs. 1.71) than P1 (phase 0.2). The MISO reported flux levels are more than 1 order of magnitude higher than the next highest points (those from Comptel) and are inconsistent with extrapolations from either the *ASCA* or Comptel spectra. Furthermore, the MISO points range in significance from 1 to 2 σ and thus should be treated as upper limits.

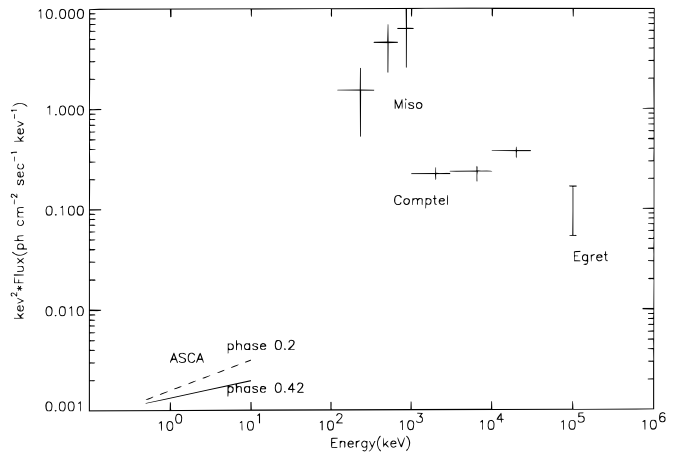

FIG. 5.—Summary of high-energy measurements of LSI +61°303

The *ASCA* spectrum has been extrapolated to high energy for the different power-law indices and normalizations (e.g., see Table 2). The best-fit parameters for both *ASCA* pointings give spectra well below the Comptel measurements (see Fig. 5). Even the 90% upper limits are well below: i.e., the 90% upper limit to the flux at 10 MeV from the *ASCA* P1 spectrum is 0.043 keV cm^{-2} s^{-1}. However, the *ASCA* P1 spectrum does extrapolate to the *COS-B* and EGRET data: the 90% *ASCA* P1 upper and lower flux limits at 200 MeV are 0.131 and 0.026 keV cm^{-2} s^{-1}. The *ASCA* P2 spectrum 90% upper and lower flux limits at 200 MeV are 0.026 and 0.0049 keV cm^{-2} s^{-1}. The behavior as a function of orbital phase or the long-term variability of the high-energy γ-ray or of the X-ray (2–10 keV) flux is not well measured for LSI +61°303, so the possible explanation of the above discrepancy is that the measurements sample different parts of the orbital period and different orbits. Since the Comptel and EGRET data sampled a large part (2 week viewing period) of the 26 day orbit, it is more likely that the cause is orbit-to-orbit variability rather than different phase sampling at low and high energy. Without further observations, it cannot be concluded that the spectrum has an MeV bump.

The *ASCA* spectrum has also been extrapolated down in energy. Here we consider the overall spectrum of LSI +61°303 at times outside of radio outburst. The change of spectrum with binary phase is considered in the companion paper (Harrison et al. 1996), which discusses two frequency radio observations over a complete orbital cycle and simultaneous with the X-ray observations. The radio spectrum of LSI +61°303 has been determined to be flat, although the spectral index is not well constrained (Gregory et al. 1979; Taylor & Gregory 1984). A radio spectral index of 0.25 outside of radio outburst (equivalent to X-ray spectral index of 1.25) is found (Harrison et al. 1996), which is consistent with previous data. Using the mean spectral parameters for both the *ASCA* pointings, spectral index of 1.75 and power-law normalization of 1.5×10^{-3}, the predicted flux density at 1.5 cm wavelength is 205 mJy. This is within the range of observed flux densities from LSI +61°303 during outburst, but the mean observed flux density outside outburst is near 20 mJy. In order to obtain 20 mJy at 1.5 cm, a break in spectral index from 1.75 to 1.25 is required at near 200 GHz. The predicted flux density at the break frequency is 36 mJy.

4.2. *Source 2*

Source 2 has a spectrum which is likely thermal with temperature of 0.8 keV. This temperature is typical for the hot component for stellar coronal emission, for early-type star stellar wind shock emission, for supernova remnants, or for emission from a spiral galaxy. The stellar interpretations are most likely since a spiral galaxy would have a column density larger than LSI +61°303 and a supernova remnant would appear as an extended object (young compact supernova remnants would be hotter).

An attempt to identify source 2 was made. Using the NED database, the search yielded no sources coincident with source 2. It did yield three sources other than LSI +61°303 within the GIS fields of view: 4C +61.06, 87GB 023740.5+611333, and 87GB 023440.3+605537, and no other sources in the SIS fields of view. None of the three had

any excess counts in GIS2 or GIS3, with 3 σ upper limits to flux (2–10 keV) of 3×10^{-14} ergs cm^{-2} s^{-1}. A 10.9 photographic magnitude optical counterpart was found in the BD star calatalog: BD 60536, classified as G2 (Brodskaya & Shajn 1958). Goldoni & Mereghetti (1995) have used *ROSAT* observations of source 2 and also identified it with BD 60536. This confirms that source 2 is very likely a stellar coronal source; it is unlikely to have affected any of the high-energy measurements of LSI +61°303, which were made with instruments which could not resolve source 2 from LSI +61°303.

4.3. *X-Ray Emission Models for LSI +61°303*

Two basic models were proposed over a decade ago to explain the radio outburst of LSI +61°303. Maraschi & Treves (1981) postulate an interaction front between an OB star wind and the relativistic wind of a young pulsar. The relativistic electrons accelerated at the wind interaction shock front produce synchrotron radiation. The radio outbursts arise as a result of electrons radiating in a changing magnetic field at the interaction front due to an eccentric orbit. X-ray and γ-ray emission is predicted from inverse-Compton scattering of stellar photons on these same energetic electrons. Taylor & Gregory (1984) propose a model in which a compact object in a highly eccentric orbit around an OB star accretes at supercritical rates via Roche lobe mass transfer at periastron. The episodes of supercritical accretion produce energetic electrons which are observed in bursts of radio emission. Here also, inverse-Compton scattering of stellar photons gives the X-ray and γ-ray emission. More recently (Campana et al. 1995 and references therein) it has been realized that there is a third mode of interaction of a pulsar and stellar wind, i.e., accretion onto the pulsar magnetosphere. This occurs when the stellar wind ram pressure exceeds the pulsar wind pressure but is not large enough to penetrate the pulsar magnetosphere boundary.

We now discuss how the *ASCA* observations shed new light on the emission mechanisms for LSI +61°303 . Here we have shown, for the first time, that LSI +61°303 does in fact have a power-law X-ray spectrum in the 0.5–10 keV energy range, and that it extrapolates up in frequency to match the γ-ray spectrum at EGRET and *COS-B* energies. It also extrapolates down in frequency to intersect the radio spectrum at 200 GHz, where a spectral break is required. The power-law radiation luminosity is dominated by higher energy photons: the radio luminosity (1.46–200 GHz) is 5.0×10^{28} ergs s^{-1}; the radio to X-ray (200 GHz–1 keV) luminosity is 5.9×10^{33} ergs s^{-1}; the 1 to 10 keV luminosity is 4.7×10^{33} ergs s^{-1}; the 10 keV to 200 MeV luminosity is 1.2×10^{35} ergs s^{-1}. (A distance of 2.3 kpc has been assumed here.) The total nonthermal luminosity in all wavebands is about 1.3×10^{35} ergs s^{-1}. This is a serious problem for the supercritical accretion model, in which the expected luminosity is of order 10^{38} ergs s^{-1}.

The power-law radiation energy density, using the above flux estimates, in the source region is 0.002 ergs cm^{-3}, for source size of 1.5 mas (Massi et al. 1993), compared to the magnetic field energy density of 0.003 $(B/1\ \mathrm{G})^2$ ergs cm^{-3}. However, the B0 companion star provides a larger radiation density (2 ergs cm^{-3} is the mean value inside a sphere of radius equal to the mean orbital separation, for a B0 stellar luminosity of 1.3×10^{38} ergs s^{-1}), ensuring that inverse-Compton losses dominate, unless the magnetic field, B, is larger than about 26 G and much higher than the equipartition value (with the relativistic electrons) of 1 G (Massi et al. 1993). The ratio of inverse-Compton losses on stellar photons to synchrotron losses is $[26/(B/1\ \mathrm{G})]^2$.

Independent of B, for a given electron energy spectral index, the inverse-Compton and synchrotron spectra have the same spectral indices. However, a given energy of relativistic electrons produces inverse-Compton and synchrotron photons of different energies. Inverse-Compton γ-rays between 1 MeV and 200 MeV come from electrons emitting $460(B/1\ \mathrm{G})$ GHz to $92(B/1\ \mathrm{G})$ T Hz [$0.38(B/1\ \mathrm{G})$ eV] synchrotron photons. Inverse-Compton X-rays from 1 to 10 keV come from the same electrons as $460(B/1\ \mathrm{G})$ MHz to $4.6(B/1\ \mathrm{G})$ GHz synchrotron photons. The inverse-Compton spectrum has a lower cutoff at the stellar photon energy of a few eV, below which only synchrotron photons are emitted. The synchrotron spectrum has an upper cutoff or spectral break depending on the electron spectrum upper cutoff or break energy.

Consider the case of strong magnetic field ($B > 26$ G). This is not ruled out by observations, since the synchrotron self-absorption frequency is 3.7 GHz for $B = 26$ G and is thus not inconsistent with radio measurements. If the electron spectrum extends to high energy then the full power-law spectrum, radio through γ-rays, could be caused by synchrotron emission. Using a spherical source of angular size 1.5 mas (Massi et al. 1993; Taylor et al. 1992) and distance 2.3 kpc (Gregory et al. 1979), the X-ray normalization gives the product of electron energy and (magnetic field)$^{(\gamma+1)/2}$, where $\gamma = 2.5$ is the power-law index of the electron spectrum. For a magnetic field of 26 G, the integrated electron energy between 2.4 and 7.6×10^{11} eV (i.e., energy of electrons responsible for 1–10 keV photons) is 3.8×10^{34} ergs. The total energy for electrons radiating above 200 GHz up to 200 MeV is 2.9×10^{36} ergs. The main contribution is from the lower energy electrons. Electrons with energy less than 2.2×10^7 eV emit below 200 GHz. If there is a 200 GHz spectral break due to electron spectrum, the lower energy electrons have $\gamma = 1.5$ and total energy (for 1.46–200 GHz photons) of 1.1×10^{33} ergs. The other possibility is that the difference between the observed radio spectral index and the X-ray and γ-ray spectral index is because of self-absorption in the radio band. Then $\gamma = 2.5$, and the energy in low-energy electrons is much larger: 7.0×10^{36} ergs. The electron energy for X-ray to γ-ray (i.e., above 10 keV) emitting electrons ($\gamma = 2.5$) is 4.5×10^{34} ergs. For larger B, the electron energies scale as $B^{-1.35}$.

However, the electron spectrum is unlikely to extend up to the value of $3.9 \times 10^{13}/B^{1/2}$ eV necessary to give 100 MeV synchrotron photons. If we assume shock acceleration, confinement of the electrons in the acceleration region (size 1.5 mas) limits electron energy to less than $5.7 \times 10^7 B$ eV. Then the synchrotron spectrum can extend only up to $1.7 \times 10^{-4} B^3$ eV or $41B^3$ GHz. The higher energy nonthermal photons are caused by inverse-Compton emission, with an upper cutoff energy for the inverse-Compton photons of $9.2 \times 10^4 B^2$ eV. This then restricts the minimum magnetic field to 33 G to yield 100 MeV photons. The above discussion on electron energies is still valid for the low-energy electrons. The high-energy inverse-Compton photons and radio synchrotron photons come from the same electrons, and there is no population of high-energy electrons. The lack of an observed spectral break between 1 keV and 200 MeV for the inverse-Compton radiation implies the emitted synchrotron spec-

trum does not have a break or cutoff between 4.6(B/1 G) MHz to 92(B/1 G) T Hz [or 0.38(B/1 G) eV]. In particular, the spectral break required between X-ray and radio should not be caused by electron spectrum break but rather by self-absorption. The intrinsic radio spectral index is 1.75, with the observed radio spectral index of 1.25 in the 1.4–5 GHz band caused by self-absorption. This is consistent since the predicted frequency where self-absorption sets in is the middle of the observed band of radio frequencies: 2(B/1 G)$^{0.2}$ GHz, using the VLBI-measured angular size of LSI +61°303 (Massi et al. 1993).

The above discussion shows that the sub-eV (radio) spectrum should be synchrotron in origin, and the super-eV (X-ray to γ-ray) spectrum should be inverse Compton in origin. The upper energy to the synchrotron spectrum is because of the limits of the particle acceleration. In this case, from the known synchrotron and inverse-Compton emissivities from a relativistic electron population, there is a single value of magnetic field which gives both the observed radio and X-ray fluxes. This value is 300 G, and the resulting electron spectrum is of the form $3.0 \times 10^4 E^{-2.5}$ cm^{-3}. Here we have assumed that the same population of electrons produces both the high-energy and the radio emission. We have also taken the electron density and magnetic field to be uniform, so the values for both are average values in the emission region.

In the case of low magnetic field ($B < 26$ G), the radio and X-ray emission come from two different populations of electrons. In addition, the radio emitting electrons must be far from or shielded from the Be star to avoid strong inverse-Compton losses. We do not consider such a complicated situation here.

In summary, the main features of the radio to γ-ray spectrum of LSI +61°303 agree with an inverse-Compton plus synchrotron model. The radiation above eV energies is inverse-Compton in origin; that below eV energies is synchrotron. A high magnetic field of about 300 G is required to give the observed radio and X-ray fluxes. The difference in spectral index in the observed radio band (1.25) and in the high-energy bands (1.75) is caused by self-absorption, which sets in at a frequency near 6 GHz. The X-ray and radio emission both originate in radiation from relativistic electrons and are therefore related to the mechanism for energetic particle production in LSI +61°303. Discussion of what particle production mechanism is appropriate to LSI +61°303 is dependent on what is known about the variation of both radio and X-ray emission with orbital phase. This is discussed together with the time-variability analysis of the *ASCA* data in Harrison et al. 1996.

5. CONCLUSION

The *ASCA* observation of LSI +61°303 has provided a high-quality spectrum for the first time. The spectrum is of power-law form, with index 1.6–1.9, and the column density to LSI +61°303 is determined accurately as $5.5–6.5 \times 10^{21}$ cm^{-2}. There is evidence for spectral steepening by 0.12 in index between phase 0.2 and 0.42, coincident with a decrease in 2–10 keV X-ray flux by 30%. The low X-ray luminosity and the upper limit on iron line emission are indicators that LSI +61°303 is not a classical accreting X-ray pulsar.

We have examined the Comptel, *COS-B*, and EGRET γ-ray data. The *ASCA* power-law spectrum extrapolates to high energy. It lies below the Comptel data points at a few MeV but is in agreement with the *COS-B* and EGRET data near 200 MeV.

The X-ray to γ-ray power-law spectrum can be explained by an inverse-Compton plus synchrotron model. Self-absorption results in an the observed radio spectral index different than the X-ray to γ-ray index. If the relativistic electrons are shock accelerated, the magnetic field must be larger than 30 G to produce the observed 100 MeV radiation. A magnetic field of about 300 G is derived from matching the observed X-ray and radio fluxes to the inverse-Compton plus synchrotron model.

D. A. L. acknowledges support from the Natural Sciences and Engineering Research Council. F. A. H. acknowledges support from a Robert A. Millikan Research Fellowship.

REFERENCES

Bignami, G., et al. 1981, ApJ, 247, L85
Brodskaya, E. S., & Shajn, P. F. 1958, Izv. Krymsk. Ap. Obs., 20, 299
Campana, S., Stella, L., Mereghetti, S., & Colpi, M. 1995, A&A, 297, 385
Frail, D., & Hjellming, R. 1991, AJ, 101, 2126
Goldoni, P., & Mereghetti, S. 1995, A&A, 299, 751
Gregory, P., & Taylor, A. 1978, Nature, 272, 704
Gregory, P., et al. 1979, AJ, 84, 1030
Harrison, F., & Leahy, D. 1996, in preparation
Harrison, F., Leahy, D., & Waltmann, E. 1996, ApJ, submitted
Hutchings, J., & Crampton, D. 1981, PASP, 93, 486
Maraschi, L., & Treves, A. 1981, MNRAS, 194, 1P
Massi, M., Paredes, J., Estalella, R., & Felli, M. 1993, A&A, 269, 249
Perotti, F., et al. 1980, ApJ, 239, L49
Schlegel, E., et al. 1993, ApJ, 407, 744
Spitzer, L. 1978, Physical Processes in the Interstellar Medium (New York: Wiley)
Swanenburg, B., et al. 1981, ApJ, 243, L69
Tanaka, Y., Inoue, H., & Holt, S. 1994, PASJ, 46, L37
Taylor, A., & Gregory, P. 1984, ApJ, 283, 273
Taylor, A., Kenny, H., Spencer, R., & Tzioumis, A. 1992, ApJ, 395, 268
Taylor, A., Young, G., Peracaula, M., Kenny, H., & Gregory, P. 1996, A&A, 305, 817
Thompson, D., et al. 1995, ApJS, 101, 259
van Dijk, R., Bloemen, H., Hermsen, W., et al. 1993, in AIP Conf. Proc. 304, Proc. 2d Compton Symp. (New York: AIP), 324